

Theoretical and experimental investigation on disc spring isolation system with loading rings

Kaiqiang Ma, Ying Zhou*, Decheng Lu

State Key Laboratory of Disaster Reduction in Civil Engineering, Tongji University, Shanghai, 200092, China



ARTICLE INFO

Keywords:

Disc spring

Isolation

Vertical cyclic loading tests

Loading rings

Numerical solution method

ABSTRACT

A novel disc spring isolation system (DSIS) design for buildings is proposed to isolate vibrations in the vertical direction. The system with nonlinear stiffness consists of disc springs and loading rings that reduce the influence of Coulomb friction between multiple disc springs. Theoretical analysis was first applied to establish a four-curve (FC) model to describe the force-displacement relation of DSIS by considering the influence of slip behavior and Coulomb friction between the loading rings and disc springs. Then, a series of vertical cyclic loading tests were carried out to study the different mechanical properties of DSIS with or without loading rings, and the effectiveness of the loading rings was verified. By comparing with the test results, the accuracy of the proposed FC model was verified. Then, the numerical solution method using the proposed FC model to solve the dynamic response of the single degree of freedom (SDOF) system was investigated. The nonlinear transfer function curves of DSIS with loading rings were compared with those of DSIS without loading rings by numerical analysis. Finally, the comparison study of SDOF for DSIS under the specific harmonic and train-induced vibration was carried out as a case study. The comparison shows that DSIS with loading rings more effectively reduces the start frequency of the isolated system, revealing the significant advantages of adopting DSIS with loading rings in vertical isolation.

1. Introduction

Traditional base isolation technology usually focuses on the vibration in the horizontal direction. However, in some cases, vibrations in the vertical direction such as earthquakes and train-induced vibrations in the cities should not be ignored.

Many studies have shown that vertical earthquakes should not be ignored in the design and analysis process due to their influence on component forces. The maximum axial load of columns could be significantly increased by the vertical component of an earthquake [1]. The vertical damping ratio should be estimated considering the vertical earthquake motion when the analysis and design of structures were carried out [2,3]. Based on the observational and analytical evidence, the importance of including vertical motion in earthquake-resistant design and analysis was demonstrated [4].

Along with the development of the urban rail transit system, the train-induced vibration which is usually an important influence part of comfort in urban life gets increasing attention in metro cities. The most influential component of the train-induced vibration is in the vertical

direction [5,6]. Many researchers paid attention to the influence of vibration on the over-track buildings that were built above the train track lines by the in-situ test. An in-situ test to investigate the train-induced vibration characteristics of Shanghai Metro Line 11 showed a frequency range of 10Hz–240Hz [7,8]. Some studies have shown that the vibration level of train-induced vibration could exceed the limit in the code in some cases [9,10]. To reduce the damage caused by vertical earthquakes and improve the residential comfort of the buildings subjected to train-induced vibrations, it is necessary to study the vertical isolation of buildings.

Unlike isolation in the horizontal direction, isolation in the vertical direction should take into account the gravitational load that must be sustained by the isolators. An effective isolation system should be of sufficient flexibility to meet the various loading capacity requirements in the vertical direction. Existing studies have shown the feasibility and difficulty of vertical vibration isolation. The linear low-stiffness vertical isolation system may lead to large initial settlements due to the self-weight of isolated buildings, and earthquakes with high-intensity or low-frequency components have large isolation drift [11]. The

* Corresponding author.

E-mail addresses: mkqtj@tongji.edu.cn (K. Ma), yingzhou@tongji.edu.cn (Y. Zhou), ludecheng@tongji.edu.cn (D. Lu).

preceding problems are obstacles to the development of vertical isolation systems for buildings.

To have vertical isolation performance, a linear stiffness system using coil springs was proposed early [12,13]. By increasing the thickness of the rubber layer, thick rubber bearings were studied in vertical isolation. Many studies on thick rubber bearings have shown that thick rubber bearings can reduce train-induced vibration to a certain extent [14,15]. However, due to the material characteristics of rubber, the isolation efficiency of thick rubber bearings is limited. Thick rubber bearings is a linear isolation system with conflicting stiffness requirement in the vertical direction, which cannot achieve an effective isolation effect. To overcome this limitation, nonlinear springs have been used to obtain high static stiffness and small dynamic stiffness, resulting in low start frequencies [16,17]. In recent years, the use of the nonlinear system to isolate vibration has received increasing attention [18–20]. By combining linear coil springs in an inclined form, a quasi-zero-stiffness system that can make the dynamic stiffness close to zero has been widely studied [21–23]. By changing coil springs into other types of springs such as plate springs, the quasi-zero-stiffness system with different forms was studied [24]. Using the geometric nonlinearity of the disc springs, a vertical isolation system with high static and low dynamic stiffness properties is established by using a single disc spring, which has been studied by many researchers [25–28]. In addition, many scholars have paid attention to the isolation system by using combined disc springs directly. These studies show that disc springs with significantly nonlinear stiffness can easily obtain high static and low dynamic stiffness characteristics. Therefore, the isolator consisting of disc springs will have an effective isolation ability. Since disc springs can be flexibly combined and can easily meet the resistance capacity requirements of isolation systems, the use of disc springs to isolate the vertical vibration was widely considered [29–32]. However, the effect of Coulomb friction between multiple disc springs is usually not considered.

DSIS is an isolation system composed of single or multiple pieces of disc springs that are arranged in parallel or in series. However, the actual isolation effect of traditional disc spring combinations is usually much lower than expected, as a result of the influence of Coulomb friction. When multi-piece disc springs are connected in parallel, the large area of surface contact between the disc springs will significantly affect the resistance by Coulomb friction, resulting in a large transition stiffness from loading to unloading [33,34]. Because the transition stiffness closely relates to the start frequency of the isolation system, the isolation efficiency of DSIS will be reduced due to too excessive Coulomb friction force.

To consider the mechanical influence of the Coulomb friction on DSIS, an FC model was proposed. In order to solve the problem of Coulomb friction for DSIS, a novel combination type with loading rings between disc springs is presented in this paper for the first time. The loading rings can convert the surface contact between disc springs into a line contact between the disc springs and the loading rings. The change of contact mode will greatly reduce the influence of Coulomb friction force on DSIS, enabling DSIS with loading rings to achieve higher isolation efficiency.

This paper mainly focuses on the comparison of DSIS with or without loading rings. Firstly, the constitution of DSIS with or without loading rings is introduced. The DSIS with loading rings is theoretically studied, and the FC model considering the influence of Coulomb friction and slippage is established. Secondly, to evaluate the effect of loading rings, a series of cyclic loading tests were performed on DSIS. By comparing the test results of the transition stiffness from loading to unloading of DSIS with or without loading rings, the effectiveness of loading rings in reducing the Coulomb friction force of DSIS is verified. And based on the test results, the accuracy of the FC model is also confirmed. A numerical solution method for solving the SDOF system with DSIS was also studied. Finally, the transfer function curves and isolation effects of the DSIS with or without loading rings are compared. The comparison shows that the start frequency of DSIS with loading rings is lower than that of DSIS

without loading rings, and DSIS with loading rings had a better isolation efficiency than that of DSIS without loading rings.

2. DSIS design concept

2.1. Mechanical properties of disc spring

Disc springs with nonlinear stiffness could well fit the concept of high static and low dynamic stiffness, which will give the isolator composed of disc springs good isolation performance. The schematic diagram of the single disc spring and its cross-sectional view is shown in Fig. 1. The parameters and loading positions of the single disc spring used in this study are defined in Fig. 2a, and the schematic diagram of deformation under vertical force is shown in Fig. 2b. Under the action of vertical force, the deformation of disc spring is x , represented by the dotted line in Fig. 2b. As x increases, the reaction force of the disc spring increases nonlinearly, while the stiffness of the disc spring decreases nonlinearly, which can provide better isolation efficiency than conventional linear isolator.

The resistance of the disc spring F_d can be expressed by a third-order equation as follows [25,35].

$$F_d = \frac{2\pi Ex}{(d_1 - d_2)^2(1 - \mu^2)} \left\{ \left[\frac{1}{2}(d_1^2 - d_2^2) - \frac{(d_1 - d_2)^2}{\ln(d_1/d_2)} \right] \times \left(\frac{h}{r_1 - r_2} - \frac{x}{d_1 - d_2} \right) \left(\frac{h}{r_1 - r_2} - \frac{x}{2(d_1 - d_2)} \right) t + \frac{t^3}{12} \ln \frac{d_1}{d_2} \right\} \quad (1)$$

where d_1 and d_2 are the distances between the central axis and the lower and upper load point; r_1 and r_2 are external and internal radii; h is the height of the inner cone; t is the thickness of the disk spring; E is the elastic modulus of the material; μ is the Poisson ratio of the disk; x is the deformation of the disc spring relative to its original state.

Simplify Eq. (1) to obtain the following equation:

$$F_d = \frac{Ex}{d_1^2(1 - \mu^2)} \left[(\bar{h} - x) \left(\bar{h} - \frac{x}{2} \right) \frac{t}{M} + \frac{t^3}{N} \right] \quad (2)$$

where \bar{h} is the effective height of the disc spring, which is defined as:

$$\bar{h} = h \frac{d_1 - d_2}{r_1 - r_2} \quad (3)$$

C , M , and N are the loading position parameters, which are defined as:

$$C = \frac{d_1}{d_2} \quad (4)$$

$$\frac{1}{M} = \pi \left(\frac{C+1}{C-1} - \frac{2}{\ln C} \right) \left(\frac{C}{C-1} \right)^2 \quad (5)$$

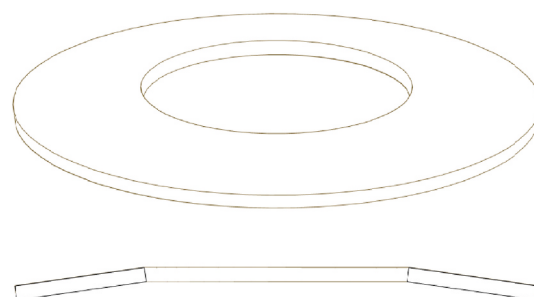


Fig. 1. Three-dimensional and cross-sectional schematic diagram of disc spring.

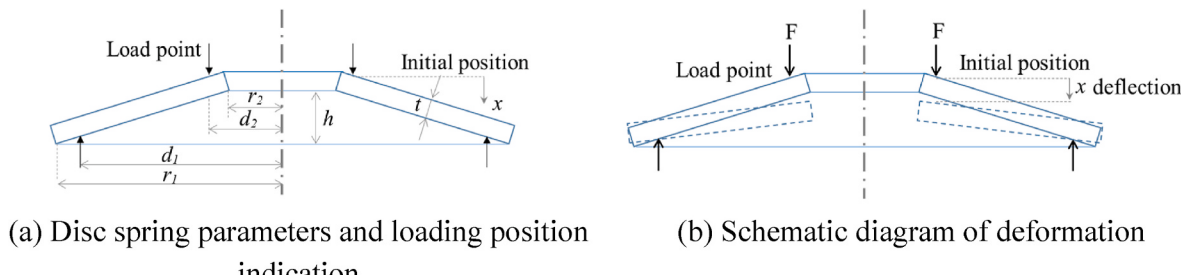


Fig. 2. Schematic diagram of disc spring.

$$\frac{1}{N} = \frac{\pi}{6} \left(\frac{C}{C-1} \right)^2 \ln C \quad (6)$$

By deriving the displacement x in Eq. (2), the stiffness of disc spring K can be obtained:

$$K = F'_d = \frac{E}{d_1^2(\mu^2 - 1)} \left\{ \frac{t(3\bar{h} - 2x)x}{2M} - \left[\frac{t^3}{N} + \frac{t(\bar{h} - x)(2\bar{h} - x)}{2M} \right] \right\} \quad (7)$$

The height-to-thickness ratio of the disc spring is an important factor affecting the nonlinear performance, which is defined as follows:

$$r = \frac{h}{t} \quad (8)$$

Through Eq. (2) and Eq. (7), the relationship between force and displacement, as well as stiffness and displacement can be obtained. The effect of r on force-displacement and stiffness-displacement are shown in Fig. 3 and Fig. 4. As the height-to-thickness ratio increases, the degree of nonlinearity of the disc spring gradually increases, and the minimum stiffness of the disc spring gradually changes from positive to negative. Therefore, by selecting a disc spring with a reasonable height-to-thickness ratio, a DSIS with a minimum stiffness value close to zero can be obtained. Since there is no negative stiffness, problems caused by negative stiffness, such as problems in numerical unstable solutions, can be avoided. Therefore, DSIS will be conducive to engineering applications.

2.2. Mechanical properties of DSIS

When a piece of disc spring cannot meet the needs of the isolator, the common method is to combine the disc springs in parallel or series. The combination of disc springs is shown in Fig. 5. Assuming that the force of the combined disc spring in parallel and the displacement of the combined disc spring in series are uniformly distributed on each disc spring, the calculation formula of the DSIS resistance F_D can be obtained as follows.

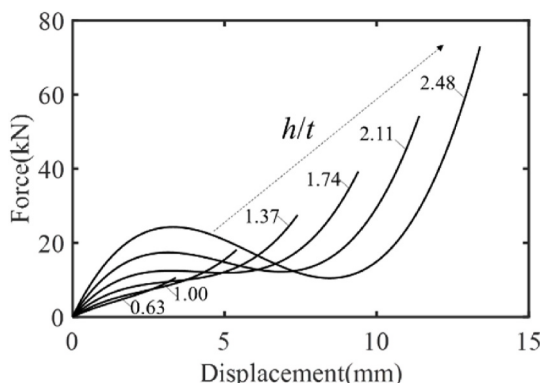


Fig. 3. Force-displacement of disc spring.

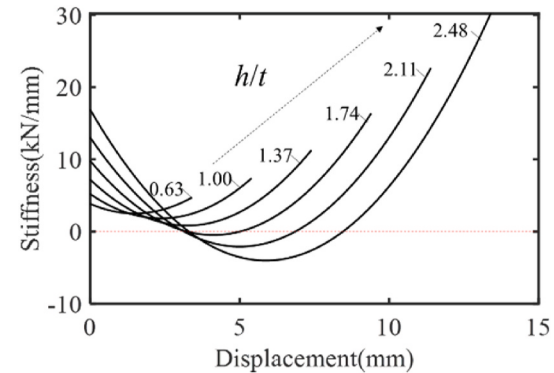


Fig. 4. Stiffness-displacement of disc spring.

$$F_D = \frac{mE(x/n)}{d_1^2(1 - \mu^2)} \left[(\bar{h} - (x/n)) \left(\bar{h} - \frac{(x/n)}{2} \right) \frac{t}{M} + \frac{t^3}{N} \right] \quad (9)$$

where m is the number of disc springs in parallel; n is the number of disc springs in series.

The influence of parameters m and n on the force and stiffness performance of the DSIS are shown in Fig. 6 and Fig. 7. With the increase of m , the resistance and stiffness of DSIS increase under the same deformation. With the increase of n , the stiffness of DSIS decreases, while the deformation capacity increases at the same time. The disc springs can be combined in any number, allowing DSIS to obtain flexible mechanical properties to suit various engineering needs.

2.3. DSIS with loading rings

The loading rings are set between the disc springs, which have the same center, as shown in Fig. 8. Small diameter loading ring is arranged in the internal position, while the large diameter loading ring is arranged in the outer position. If friction could be neglected, DSIS will have excellent mechanical properties. However, when disc springs are combined in the traditional way shown in Fig. 9, the DSIS may be heavily influenced by the Coulomb friction, resulting in large deviations from the theory. Thus, traditionally combined DSIS will achieve lower isolation efficiency than ideally. To bring the mechanical properties of DSIS close to its ideal state, DSIS with loading rings is studied below.

The friction force mechanism of traditional DSIS and DSIS with the loading rings is shown in Fig. 9. After setting the loading rings between the parallel disc springs, the friction force $A4$ can be converted to $B4 \sim B7$, which means that the surface contact friction force has been replaced by the line contact friction force. In addition, elastic slippage between the loading rings and the disc springs is more likely to occur, which will help reduce the effect of Coulomb friction. If the loading rings are set between the disc springs when the disc spring is combined in series, the maximum deformation will be enhanced. The maximum deformation of DSIS with loading rings will be enhanced to $2h + \Delta$, where

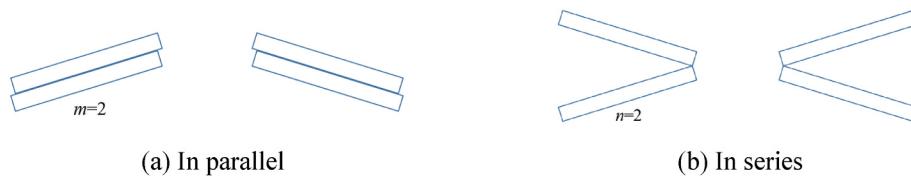


Fig. 5. Schematic diagram of combined disc springs.

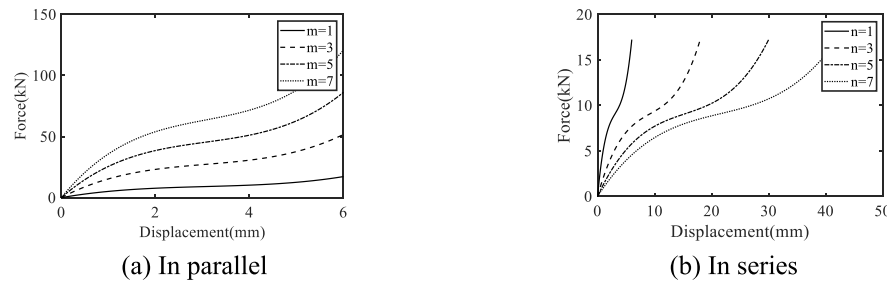


Fig. 6. Force-displacement of DSIS

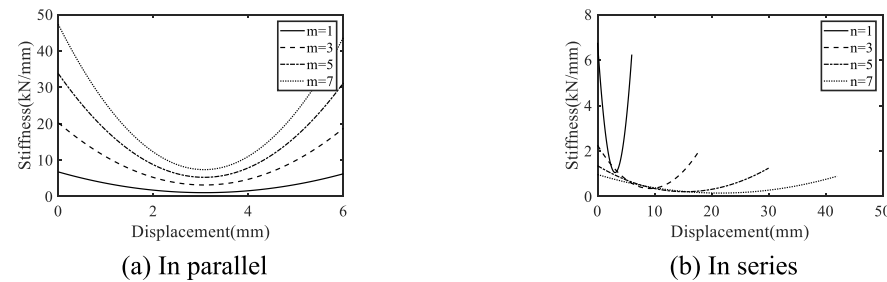


Fig. 7. Stiffness-displacement of the DSIS



Fig. 8. Setting of loading rings.

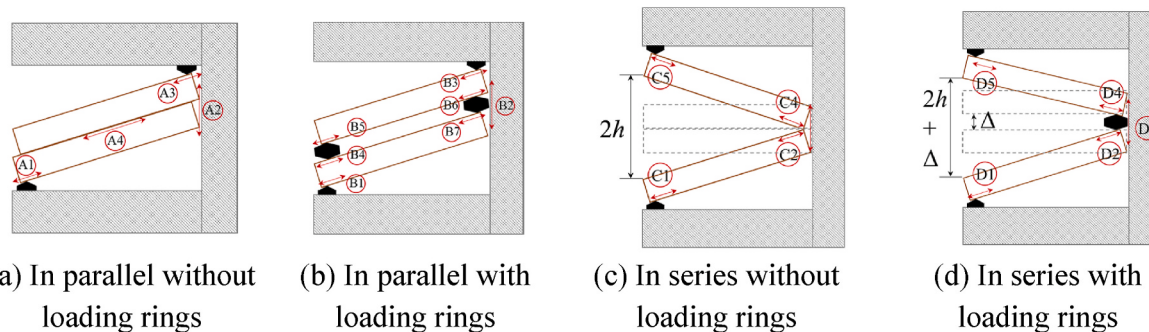


Fig. 9. The friction force mechanism of DSIS.

the Δ is the sectional height of the loading rings. As shown in Fig. 9c and d, the DSIS without loading rings can no longer be deformed, while the disc is flattened which appears as a dotted line. But the DSIS with

loading rings may have an additional deformation Δ , while the disc is flattened too.

The construction form of the typical DSIS is shown in Fig. 10. The

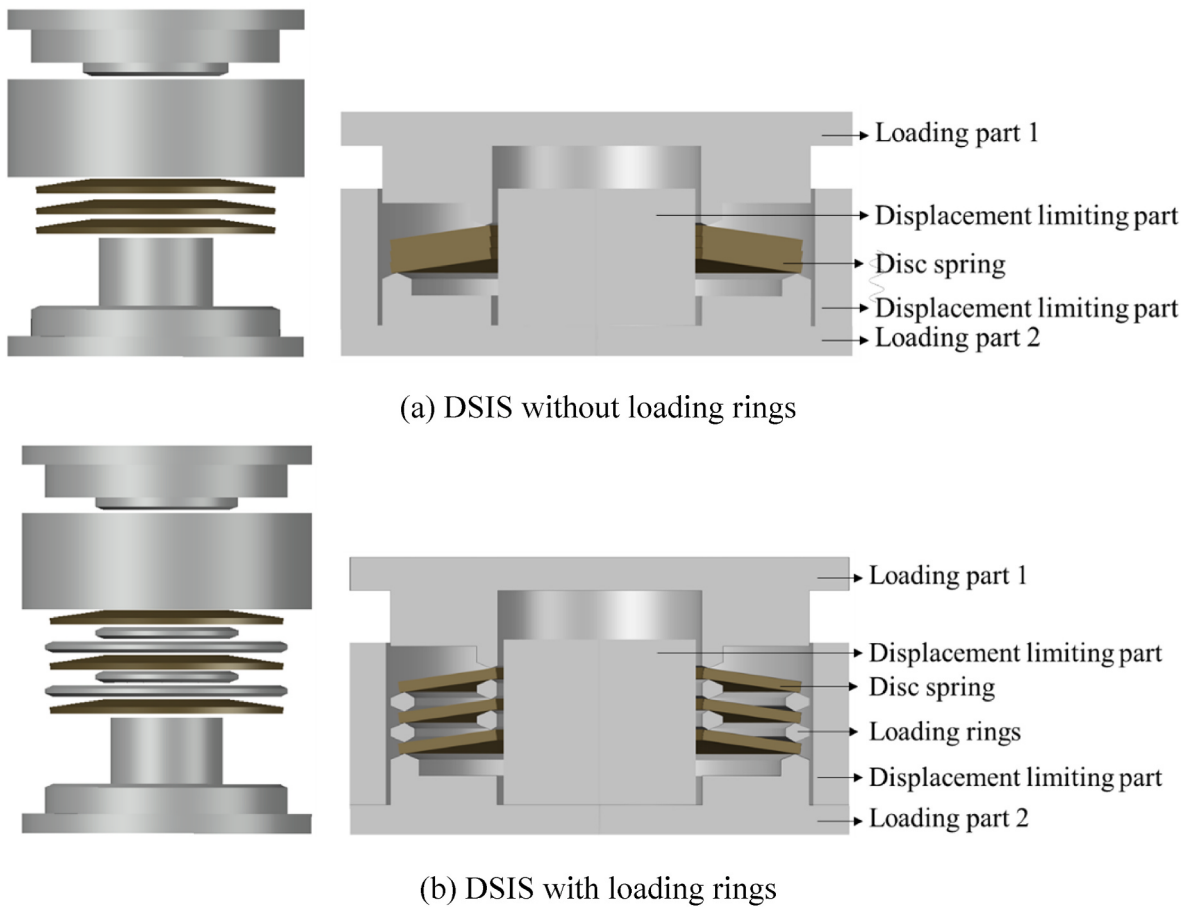


Fig. 10. Construction form of the typical DSIS.

traditional DSIS consists of disc springs, a loading part, and a displacement-limiting part. The DSIS with loading rings is shown in Fig. 10b. As for the isolator presented in Fig. 10, the isolation object is attached to the loading part 1. The ground vertical vibration transmitted from loading part 2 to the isolation object will be isolated by DSIS.

3. Theoretical research on DSIS

This section will study the force-displacement relationship of DSIS while the friction force is considered. Since the traditional DSIS is affected by Coulomb friction, the general form of the compression hysteresis curve is shown in Fig. 11a [36]. The DSIS with loading rings can reduce the friction area at the contact position. When the state of DSIS is from loading to unloading, the slip between the loading ring and the disc

spring will cause more deformation of the friction release, thus making the resistance change smoother than that of DSIS without loading rings. Therefore, based on Fig. 11a, the compression hysteresis curve of DSIS with loadings rings is assumed to be a new form by extending the loading length to the unloading, as shown in Fig. 11b, which is also verified in later tests. Curves AB and CD represent loading and unloading resistance, respectively. Curve BC is the transition from loading to unloading, while curve DA is the transition from unloading to loading. Under the influence of Coulomb friction, the resistance of DSIS increases under loads such as curve AB and AtBt, and decreases during the unloading such as CD and CtDt. By setting the loading rings between the disc springs, the transition stiffness K_{ul} will be less than K_{tul} , and the length of the transition will be longer than that of traditional DSIS. Meanwhile, the equivalent stiffness of DSIS with loading rings becomes

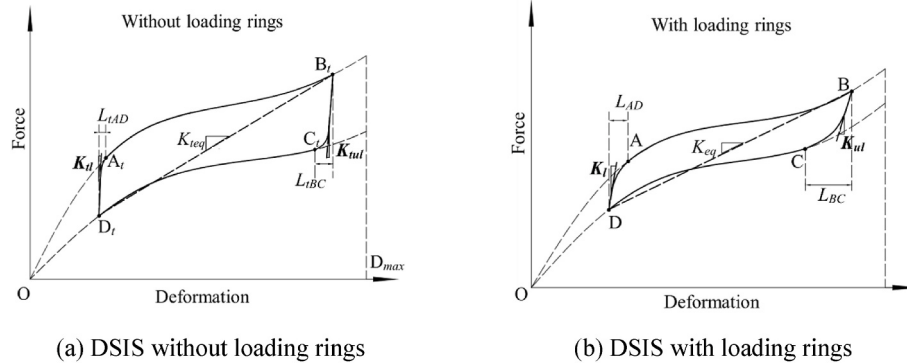


Fig. 11. Compression hysteresis curve of DSIS.

smaller due to the reduced friction.

3.1. Resistance of disc springs under friction force

After considering the effects of friction in traditional DSIS, the loading and unloading curve of the disc spring can be calculated by the following equation [37].

$$F_T = F_D \cdot \frac{m}{1 \pm f_m(m-1) \pm f_R} \quad (10)$$

where F_D is the resistance of the combined disc springs; f_m and f_R are the coefficients of friction in parallel and series respectively; m is the number of disc springs in parallel.

When setting up the loading rings in DSIS, it will no longer be appropriate to use Eq. (10) to calculate the resistance of DSIS. Since the contact type between the loading rings and the disc springs is similar to that between disc springs combined in series, the effect of the friction force on the resistance of disc springs will have a similar form to Eq. (10). Simultaneously, when the loading rings is set, there is no surface contact between the disc springs, so the coefficient f_m may be zero. Considering the number of contact interfaces between the disc springs and the loading rings, the following equation can be obtained, and the effect of the friction coefficient is shown in Fig. 12.

$$F_R = F_D \cdot \frac{1}{1 \pm (n+2(m-1))f_R} = F_D \cdot \frac{1}{1 \pm (n+2m-2)f_R} \quad (11)$$

In addition to friction force, the effect of the loading rings also occurs at the load point. During the deformation of the disc springs, there is a slight change in the loading position. Therefore, the parameters d_1 and d_2 should be revised as follows.

$$d_{1re} = d_1 + \delta_1 \quad (12)$$

$$d_{2re} = d_2 + \delta_2 \quad (13)$$

Where δ_1 and δ_2 are parameters that correct d_1 and d_2 , by considering the error of loading rings and the effect of slipping between the loading rings and the disc springs. d_{1re} and d_{2re} are the distances between the modified central axis and the lower and upper loading positions, respectively.

Furthermore, based on the A-L solution, the resistance F_{re} of Eq. (9) modified by Eq. (12) and Eq. (13) will be rewritten as follows.

$$F_{re} = \frac{mE(x/n)}{d_{1re}^2(1-\mu^2)} \left[(\bar{h}_{re} - (x/n)) \left(\bar{h}_{re} - \frac{(x/n)}{2} \right) \frac{t}{M_{re}} + \frac{t^3}{N_{re}} \right] \quad (14)$$

where \bar{h}_{re} , M_{re} , N_{re} are parameters that are revised by Eq. (12) and Eq. (13) based on Eq. (3) to Eq. (6).

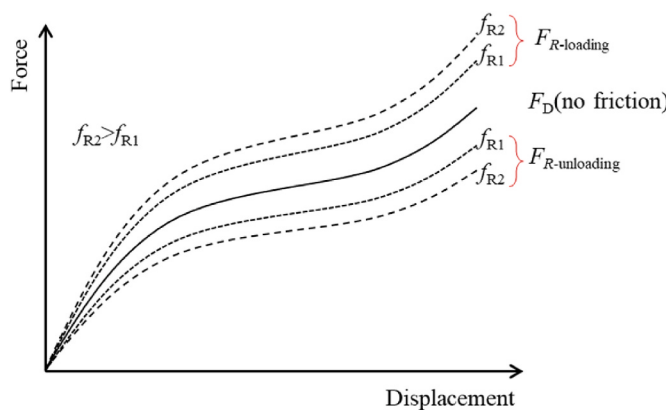


Fig. 12. Schematic diagram of friction coefficient influence.

3.2. Calculation of transition section length

The transition section is defined as the BC and DA in Fig. 11, which represents the mechanical properties of DSIS when the transition occurs between loading and unloading. Since there is no interface contact between the loading rings and the disc springs, the slippage will be more obvious. By assuming the slip mainly exists in the transition section and just occurs in the slip area shown in Fig. 13, the equation for calculating the length of the transition section can be obtained. The calculation diagram of the transition section length is shown in Fig. 13. According to the geometric relationship between the initial position and the position of the disc spring deformation x , the length of the transition section can be calculated.

$$L = \sqrt{(r_1 - r_2)^2 + h^2} = \frac{r_1 - r_2}{\cos \theta} \quad (15)$$

$$\tan \theta = \frac{h}{r_1 - r_2} \quad (16)$$

$$L_1 = \frac{r_1 - r_2}{\cos \theta} - \left(\frac{d_2 - r_2}{\cos \theta} - t \tan \theta \right) - \frac{r_1 - d_1}{\cos \theta} = \frac{d_1 - d_2}{\cos \theta} + t \tan \theta \quad (17)$$

$$L'_1 = \frac{d_1 - d_2}{\cos \alpha} \quad (18)$$

$$\sin \beta = \frac{x}{L_1} \quad (19)$$

$$\alpha = \beta - \theta \quad (20)$$

$$L_\Delta = L_1 - L'_1 + t \tan \alpha \quad (21)$$

$$L_{slip} = \eta L_\Delta \quad (22)$$

where L is the cross-sectional length of the disc spring; L_1 is the cross-sectional length of the disc springs between the two loading positions; θ is the inclination angle of the original state; α is the inclination angle when the vertical deformation of the disc spring is x ; β is the rotation angle that compares with the original state of disc spring. L'_1 is the cross-sectional length of the disc springs between the two loading positions after deformation x ; L_Δ represents the slip length between the disc spring and the loading rings; η is the correction factor which is usually taken as 1 when setting the loading rings, and if there are no loading rings, the value will be less than 1; The length of the transition section representing L_{BC} and L_{DA} in Fig. 10b will be determined based on the L_{slip} . Points C and A can be located by the length of the transition section.

Assuming that curves BC and DA have the same form of Eq. (2), the transition curve can be presented by the following polynomials.

$$F = a \cdot x^3 + bx + c \quad (23)$$

And the stiffness of the transition curve can be obtained as follows.

$$K_{tr} = F' = 3a \cdot x^2 + b \quad (24)$$

The coefficients a , b , and c can be determined according to the information at the points A to D. For example, the curve BC can be calculated by the B (F_B , x_B), C (F_C , x_C), and the stiffness of C (K_C , x_C), the accordingly system of equations as shown below.

$$\begin{cases} F_B = a \cdot x_B^3 + bx_B + c \\ F_C = a \cdot x_C^3 + bx_C + c \\ K_C = 3a \cdot x_C^2 + b \end{cases} \quad (25)$$

Based on Eq. (24) the expression of curve BC can be obtained, and DA can be obtained in the same way.

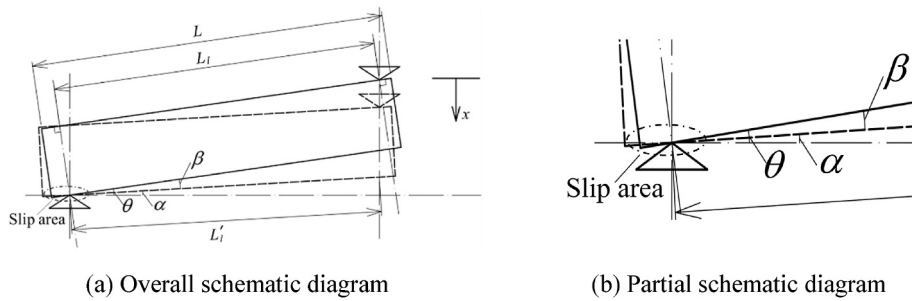


Fig. 13. Diagram of slip during the deformation.

3.3. Four-curve model

Since the influence of friction force and the transition length of DSIS have been studied, a piecewise function of the FC model describing the hysteresis curve of the DSIS can be obtained as follows.

$$F_{DSIS} = \begin{cases} \frac{F_{re-load}}{1 - (n + 2m - 2)f_{R-load}} & A \rightarrow B \\ ax^3 + bx + c & B \rightarrow C \\ \frac{F_{re-unload}}{1 + (n + 2m - 2)f_{R-unload}} & C \rightarrow D \\ \bar{a}x^3 + \bar{b}x + \bar{c} & D \rightarrow A \end{cases} \quad (26)$$

where $F_{re-load}$ and $F_{re-unload}$ are calculated by Eq. (14), and $f_{R-unload}$ have the same meaning with f_R ; a , b , c , and \bar{a} , \bar{b} , \bar{c} are determined by the information in points A to D.

This model can consider the effects of Coulomb friction and the slip at the loading position. In addition, it is easy to be used, if the four parameters f_{R-load} , $f_{R-unload}$, η , δ_1 and δ_2 are identified.

4. Experiment study of the DSIS

To study the improvement of the mechanical performance by setting loading rings, and to demonstrate the accuracy of the FC model, vertical compression reciprocating loading experiments are conducted in this section.

4.1. Information about the experiment

Various DSIS combinations with or without loading rings were designed and tested in the experiment. The parameters of disc springs used in the experiment are shown in Table 1. The height-to-thickness ratio of the disc springs for the test is about 1.3, which means the disc spring will have significant nonlinear properties but no negative stiffness. The test specimens were designed in a variety of combinations, where the configuration of 1, 3, and 5 pieces of disc springs in parallel and series were tested respectively. The specimen and its three-dimensional schematic diagram are shown in Fig. 14. The fatigue loading machine manufactured by MTS was selected for the experiment.

The loading protocol of the vertical compression reciprocating loading experiment is shown in Fig. 15. First, the disc springs are compressed to a predetermined displacement A_0 , and then the triangular reciprocating load is applied around A_0 .

The test conditions of the vertical compression reciprocating loading

experiment are shown in Table 2. To study the effects of loading amplitude and loading frequency, the variable amplitude case and the variable frequency are conducted. To investigate the effect of the loading rings, comparative tests were also carried out, in which DSIS with loading rings is in the same state as DSIS without loading rings.

4.2. Experiment results

The experiment results for each test case are shown in Fig. 16 to Fig. 17 which show that DSIS with the loading rings can significantly change the force characteristics of DSIS. The hysteresis curve of each loading cycle is consistent, indicating that the disc spring is in an elastic state during the test, and the nonlinear performance is mainly derived from geometric nonlinearity. The conclusion that the mechanical properties of DSIS vary with the change in loading amplitude can be obtained through the variable amplitude test. As the loading amplitude increases, the nonlinearity of the DSIS hysteresis curve increases. With the increasing of loading frequency, the mechanical properties of DSIS remain basically unchanged. Therefore, the mechanical properties of DSIS are basically irrelevant to the external load frequency. The beneficial effects of the loading rings can be demonstrated by comparing the results of DSIS with or without the loading rings, such as case No.3 and case No.5. The hysteresis curve area of DSIS with loading rings is smaller than that of DSIS without loading rings, which means that the damping from the Coulomb friction has been reduced substantially. The stiffness of the transition section for the DSIS with the loading rings is also significantly reduced, which can improve the isolation efficiency of DSIS.

The test results of the equivalent stiffness and equivalent damping ratio are shown in Fig. 18 to Fig. 19. Based on Eq. (27), the damping ratio can be calculated [38]. By setting loading rings between the disc springs, the equivalent stiffness and equivalent damping ratio can be significantly reduced in the test case of disc springs combined in parallel, which means that the loading rings can well change the effect of Coulomb friction. While in the test case of disc springs combined in series, the effect of Coulomb friction is not significantly reduced due to the lack of surface contact in series at the beginning. By comparing Case No.11 and Case No.13, it can be concluded that the loading rings can enhance the deformability of DSIS.

$$\xi = \frac{A_{area}}{2\pi(P_{max} - P_{min})(\delta_{max} - \delta_{min})} \quad (27)$$

where A_{area} is the area of a circle hysteresis curve; P_{max} is the maximum axial load; P_{min} is the minimum axial load; δ_{max} is the maximum relative vertical displacement corresponding to P_{max} and δ_{min} is the minimum relative vertical displacement corresponding to P_{min} .

Based on the definition of the transition section stiffness in Fig. 11, the comparison of the transition section stiffness was studied as shown in Fig. 20. The ratio at the coordinates is defined as the stiffness of DSIS with loading rings divided by the stiffness of DSIS without loading rings. By setting the loading rings, the transition stiffness from loading to unloading can be reduced to 30% of the traditional DSIS, and the

Table 1
The parameters of the DSIS (mm).

r_1	r_2	d_1	d_2	t	h
50	25.5	48.5	27.0	2.7	3.5

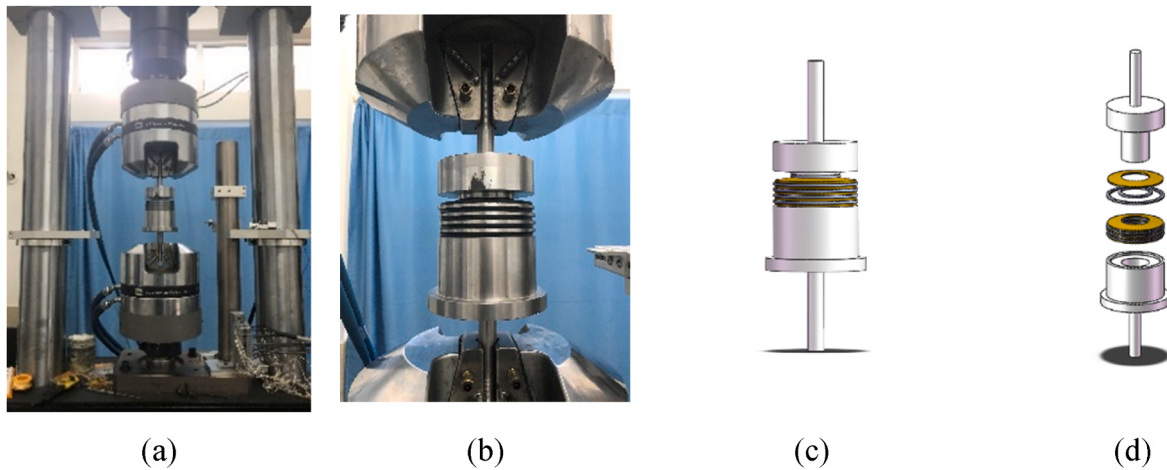


Fig. 14. DSIS used in the experiments.

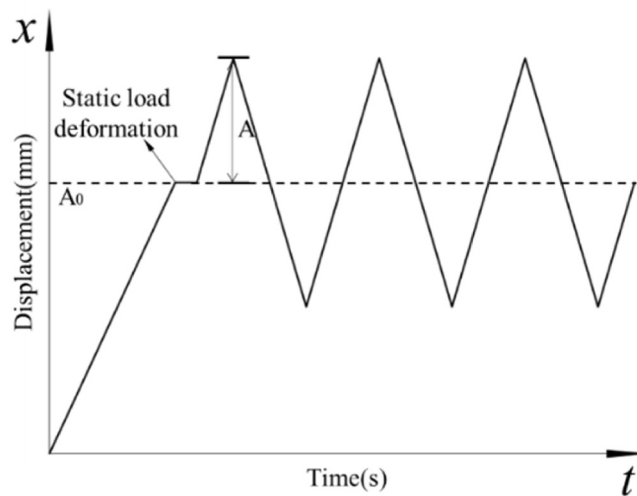


Fig. 15. Loading protocol.

Table 2
Test condition of DSIS.

Case	Loading ring	Parallel	Series	Static load position A0(mm)	Loading amplitude A(mm)	Loading frequency (Hz)
No.1	NO	1	1	3	0.5–2	0.05
No.2	NO			3	1.5	0.01–2
No.3	NO	3	1	3	0.5–2	0.05
No.4	NO			3	1.5	0.01–2
No.5	YES	3	1	3	0.5–2	0.05
No.6	YES			3	1.5	0.01–2
No.7	NO	5	1	3	0.5–2	0.05
No.8	NO			3	1.5	0.01–2
No.9	YES	5	1	3	0.5–2	0.05
No.10	YES			3	1.5	0.01–2
No.11	NO	1	3	6	1–2	0.05
No.12	NO			6	2	0.01–2
No.13	YES	1	3	9	1.5–6	0.05
No.14	YES			9	4.5	0.01–2
No.15	NO	2	3	6	1–2	0.05
No.16	NO			6	2	0.01–2
No.17	YES	2	3	9	1.5–6	0.05
No.18	YES			9	4.5	0.01–2

transition stiffness from unloading to loading could be reduced to 50% of the traditional DSIS. The reduction of the transition section stiffness can demonstrate that the setting of the loading rings provided a significantly beneficial effect on DSIS stiffness.

4.3. Comparison of theoretical model and test results

The comparison between the test results with the proposed FC model has been carried out in this section. According to Eq. (26) and Eq. (14), if the geometric parameters and combination configuration of the disc springs are selected, which means that most of the parameters required for the FC model have been determined, the hysteresis curve can be calculated while the coefficients δ_1 , δ_2 and f_R for loading part and unloading part are identified respectively. f_R is about 0.01–0.05. And the value of δ_1 and δ_2 is depending on the geometric characteristics of loading rings on the contact area. To confirm the values of δ_1 , δ_2 , and f_R , the parameter identification needs to be used, such as the least square method based on the test results. The comparison between the theoretical model and the test results is shown in Fig. 21. The test results are in good agreement with the theoretical curves calculated by the FC model, indicating that the proposed FC model can accurately describe the mechanical properties of DSIS while considering the Coulomb friction.

5. Dynamic analysis using the FC model

The dynamic analysis of SDOF using the proposed FC model is investigated in this section. The process of solving a dynamic response by stepwise integration is introduced. The case study using the proposed stepwise integration method is investigated. And the dynamic response of DSIS with or without loading rings is compared.

5.1. Process of dynamic analysis using FC model

The calculation diagram is shown in Fig. 22. Eq. (28) represents the coordinate conversion of the SDOF system. And the kinetic equation representing the i -th step can be obtained as Eq. (29), in which k represents the nonlinear stiffness of the DSIS.

$$x = v - u \quad (28)$$

$$m_0 \ddot{x}_i + c_0 \dot{x}_i + k_i x_i = -m_i \ddot{u}_i \quad (29)$$

where m_0 and c_0 are the mass and damping coefficient of the isolation object respectively.

To realize the dynamic analysis of DSIS, Eq. (26) should be rewritten to the form in Eq. (30), where the flag is used to judge the position of the

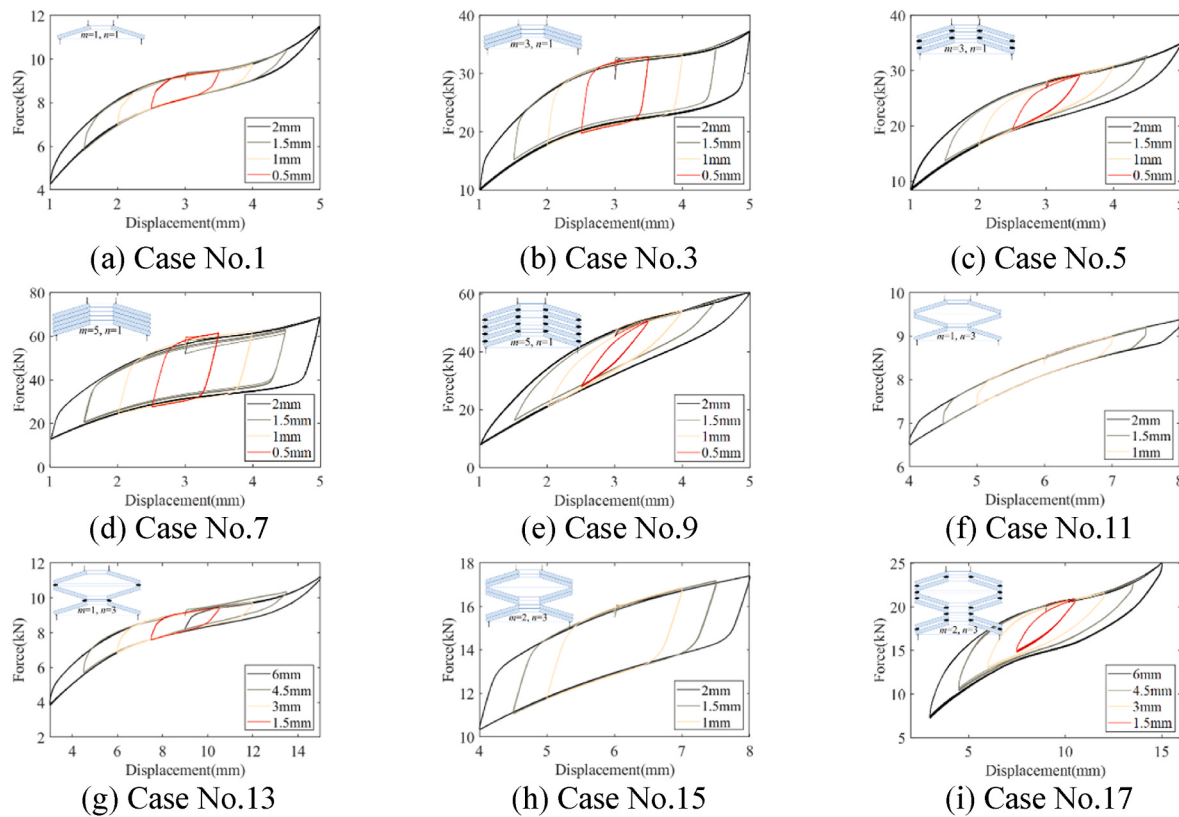


Fig. 16. Results of variable amplitude test.

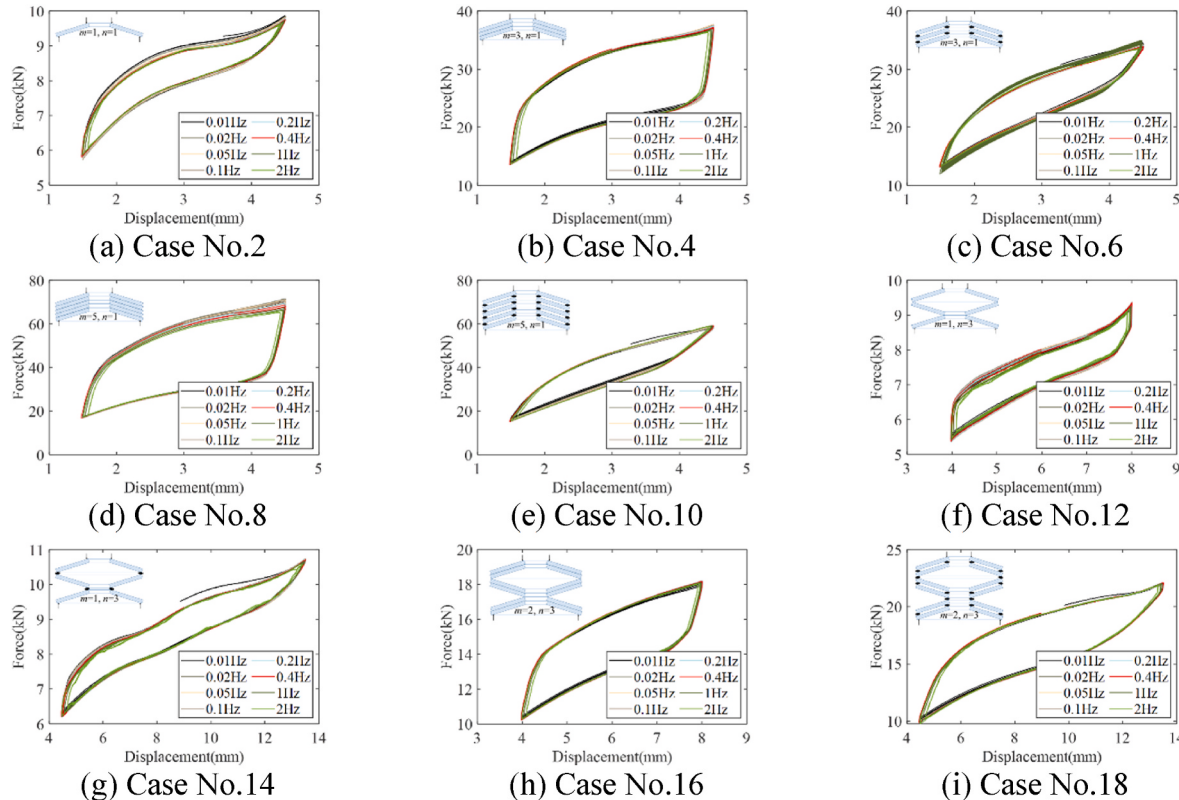


Fig. 17. Results of variable frequency test.

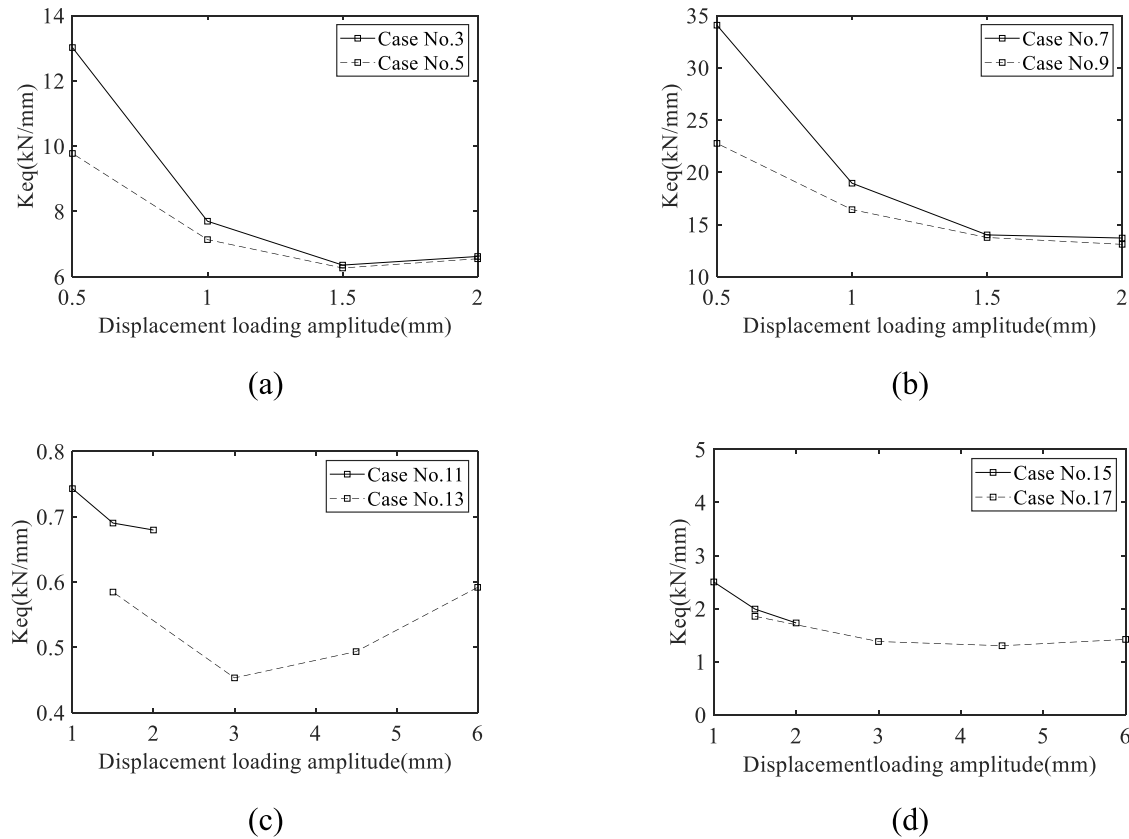


Fig. 18. The equivalent stiffness of DSIS in the test.

i -th step in the FC model. The meaning of the flag is shown in Fig. 23. According to the deformation and speed direction at the i -th step, the value of the flag can be determined. Once the value of the flag is determined, the stiffness and the resistance of the i -th step can be calculated. Then, by placing the stiffness and resistance of the i -th step into the numerical solver, the displacement, velocity, and accelerations of the $i+1$ -th step can be obtained. In addition, the new value of the flag can be determined based on the response of the $i+1$ -th step. Finally, by repeating the above steps, the dynamic response of SDOF with DSIS can be obtained.

$$F_{DSIS} = \begin{cases} \frac{F_{re-load}}{1 - (n + 2m - 1)f_{R-load}} & A \rightarrow B, \text{flag} = 1 \\ ax^3 + bx + c & B \rightarrow C, \text{flag} = 2 \\ \frac{F_{re-unload}}{1 + (n + 2m - 1)f_{R-unload}} & C \rightarrow D, \text{flag} = 3 \\ \bar{a}x^3 + \bar{b}x + \bar{c} & D \rightarrow A, \text{flag} = 4 \end{cases} \quad (30)$$

The calculation process of dynamic analysis is shown in Fig. 24. The FC model, the solving module, and the state judgement module are the most important parts of the whole calculation. The FC model is primarily used to calculate the state of DSIS. The solving module is used to calculate the next step of SDOF, in which the Newmark β method is selected. The state judgement module is used to determine the value of the flag. The calculated data circulates between these three modules until the calculation is completed.

5.2. Case study of DSIS

The parameters used to calculate the SDOF response are shown in

Table 3. For DSIS without loading rings, the coefficient η is set to 0.2, while the corresponding coefficient for DSIS with loading rings is 1.0. DSIS with or without loading rings has the same configuration. The value m_0 is based on the resistance of DSIS, and the value of c_0 is considering the Rayleigh damping ratio of about 1% of DSIS to ensure the convergence of the dynamic calculation, which is considering there is no material nonlinearity during the analysis. First, the sweep frequency signal is taken as the input to study the difference in the transfer function between DSIS with loading rings and DSIS without loading rings. The sweep frequency signal lasts for 2 s and has a spectrum range from 1 Hz to 250Hz, as shown in Fig. 25. The amplitude of the sweep frequency signal is set to 1 m/s², which is similar to the train-induced vibration [15].

The response of the DSIS with loading rings was shown in Fig. 26, and the response of the DSIS without loading rings was shown in Fig. 27. The transfer function of DSIS with or without loading rings is shown in Fig. 28. The start frequency that represents the natural frequency of the isolated system. DSIS without loading rings is about 28Hz–36Hz, while the start frequency of DSIS with loading rings is about 13Hz. According to the comparison of the two DSIS results, it can be concluded that the loading rings can significantly reduce the start frequency. By reducing the start frequency of DSIS, the isolation efficiency of the system will be significantly improved based on the basic theory of isolation.

Furthermore, a specific frequency of a harmonic wave is selected as input to demonstrate the difference between the two DSIS. A harmonic wave with 35Hz is analyzed. The analysis results are shown in Figs. 29–32. Considering the mechanical properties of DSIS are significantly affected by the loading amplitude, the analysis of different amplitudes was carried out. By comparing Fig. 29 with Fig. 31, the difference between the two DSIS can be discovered. While a small loading amplitude is inputting, the response of DSIS is mainly in the transition section, which is corresponding to the curve BC of the FC

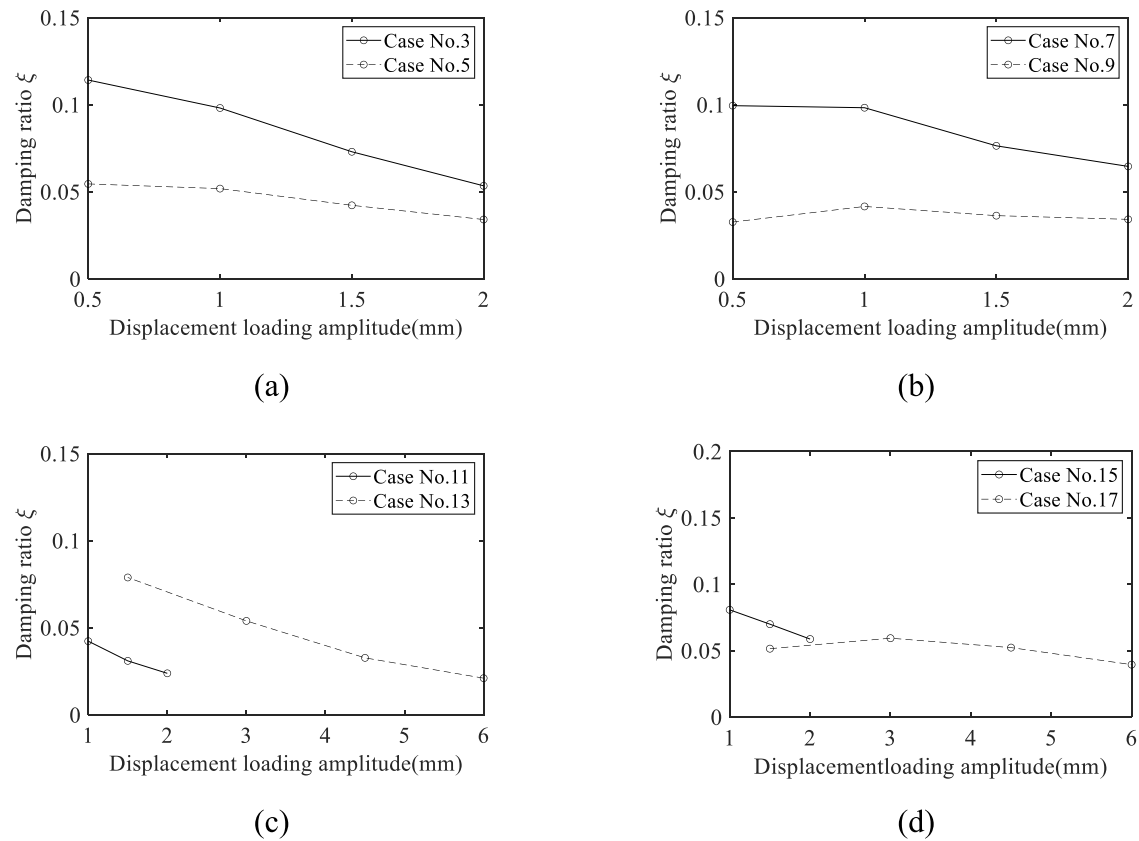


Fig. 19. The equivalent damping ratio of DSIS in the test.

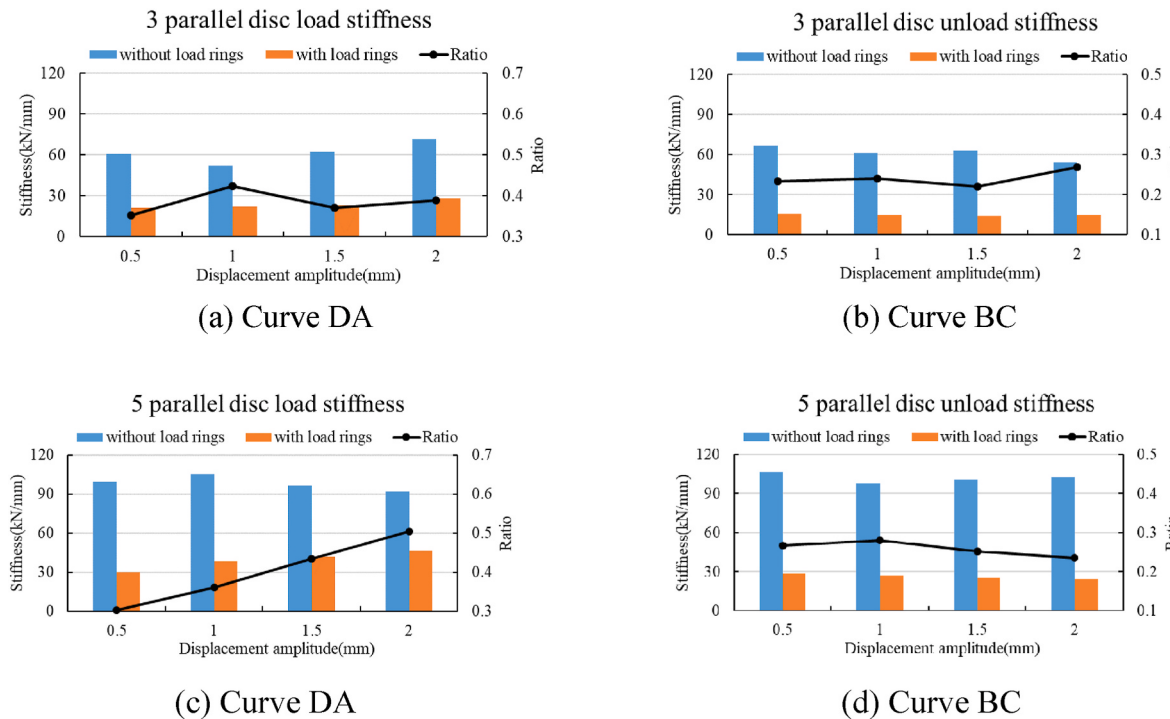
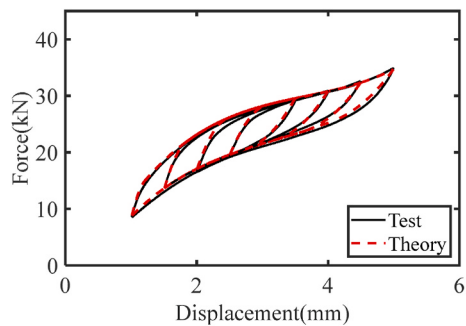


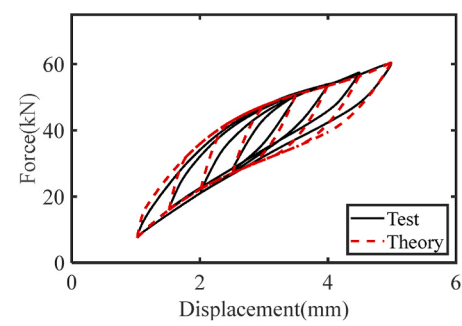
Fig. 20. Comparison of the transition section stiffness.

model. Therefore, by comparing the response of the two DSIS, the effect of the loading rings can be obtained. The input of DSIS with the loading ring can be reduced to 45%, while the DSIS without the loading rings has

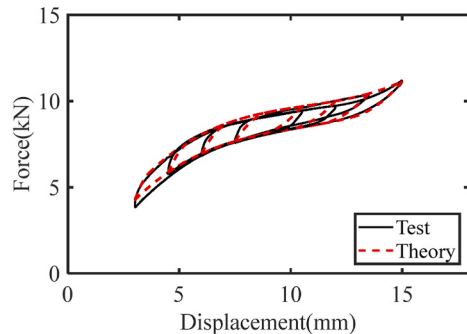
a larger response than input, which illustrates the effect of the loading rings on the transition section of the FC model. By comparing Fig. 29 with Fig. 30 and Fig. 31 with Fig. 32, the effect of the loading amplitude



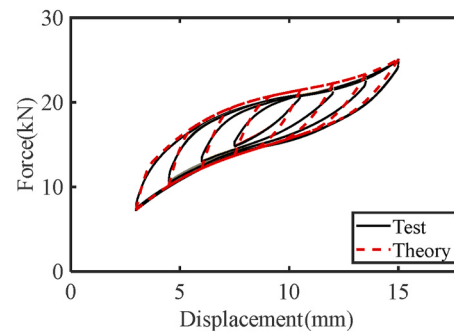
(a) Three-disc springs in parallel



(b) Five-disc springs in parallel



(c) Three-disc springs in series



(d) Two-disc springs in parallel and three-disc springs in series

Fig. 21. Comparison of test results and the theoretical curves.

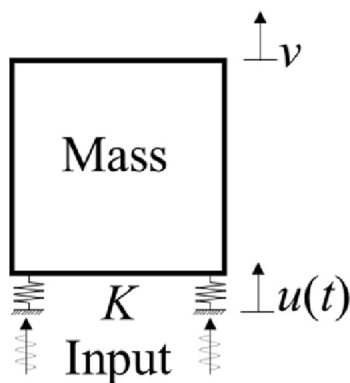


Fig. 22. Calculation diagram.

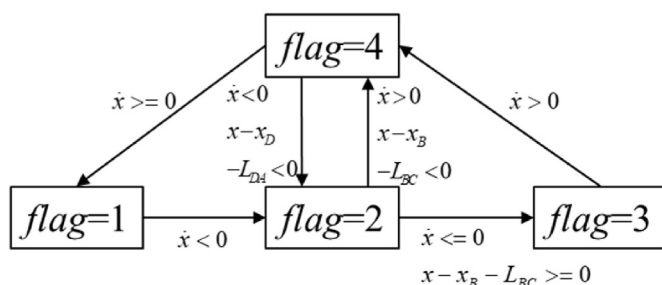


Fig. 23. Schematic diagram of flag conversion.

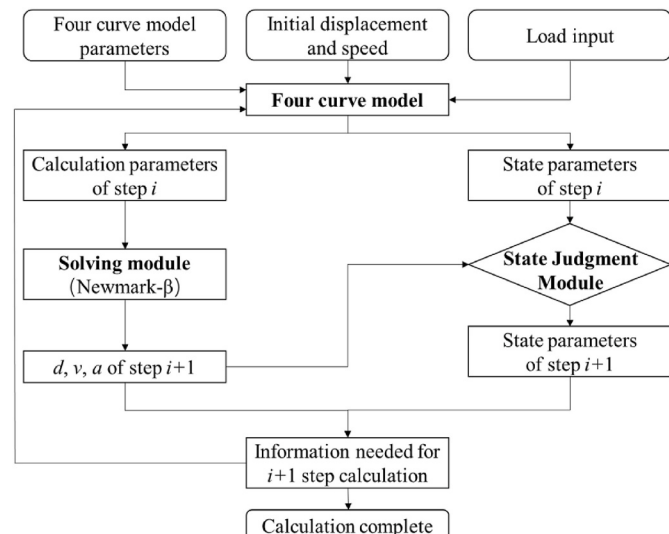


Fig. 24. Calculation flow chart.

Table 3
Parameters of the case study.

$r_1(\text{mm})$	$r_2(\text{mm})$	$d_1(\text{mm})$	$d_2(\text{mm})$	$t(\text{mm})$
50	25.5	48.5	27.0	2.7
$h(\text{mm})$	m	n	$m_0(\text{kg})$	$c_0(\text{N.s/m})$
3.5	3	1	2700	5000

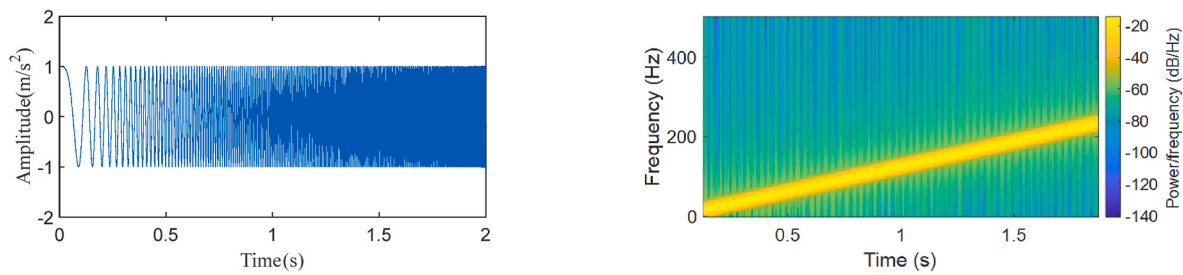


Fig. 25. Sweep frequency signal.

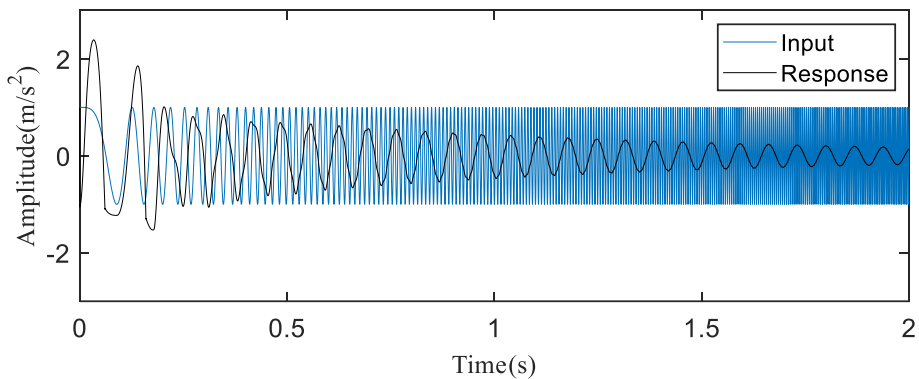


Fig. 26. The response of the DSIS with loading rings.

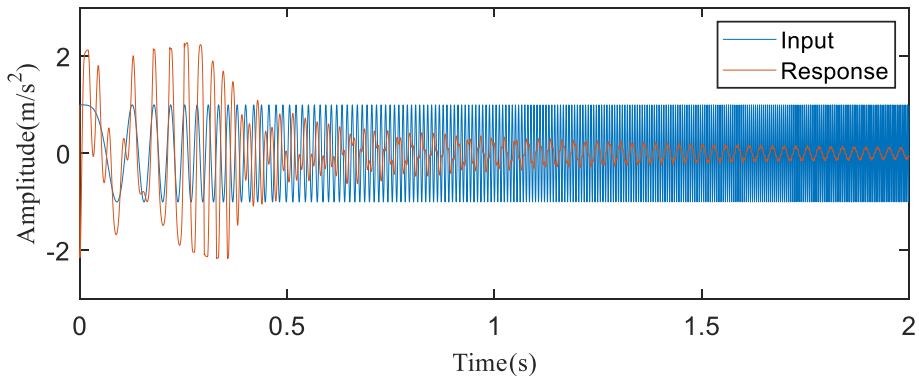


Fig. 27. The response of the DSIS without loading rings.

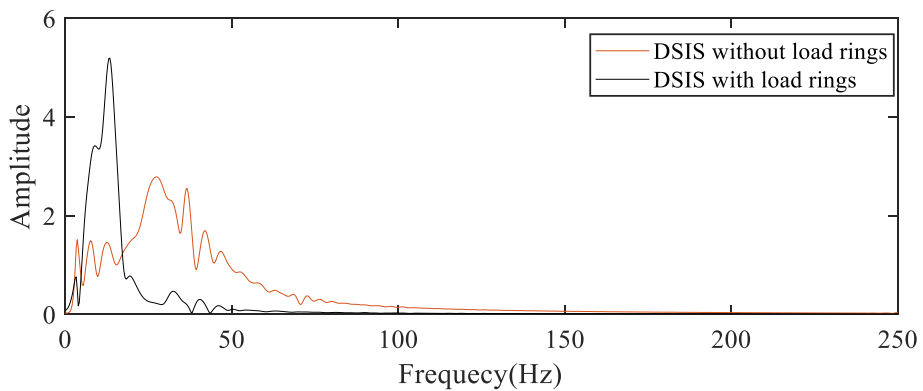
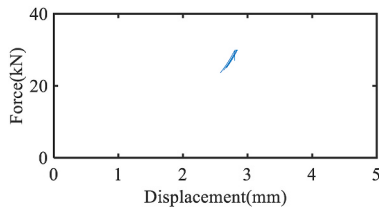
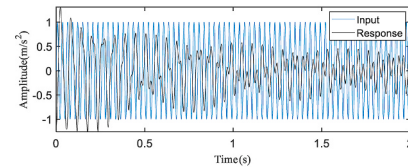


Fig. 28. Comparison of transfer function.

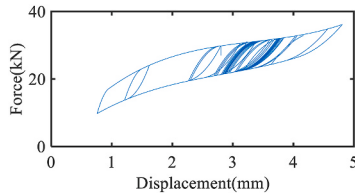


(a) Hysteresis curve

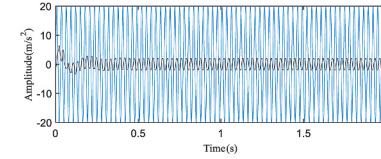


(b) Time history

Fig. 29. DSIS with loading rings at 35Hz harmonics wave with small amplitude.

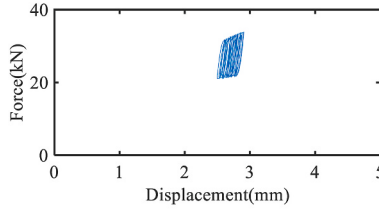


(a) Hysteresis curve

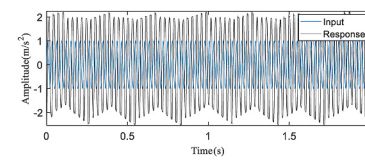


(b) Time history

Fig. 30. DSIS with loading rings at 35Hz harmonics wave with large amplitude.

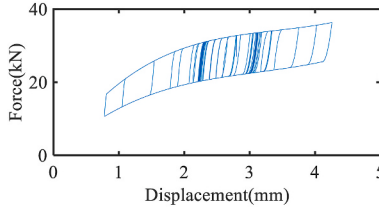


(a) Hysteresis curve

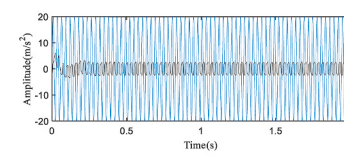


(b) Time history

Fig. 31. DSIS without loading rings at 35Hz harmonics wave with small amplitude.



(a) Hysteresis curve



(b) Time history

Fig. 32. DSIS without loading rings at 35Hz harmonics wave with large amplitude.

is studied, and when the displacement response of DSIS becomes larger, the isolation efficiency is significantly improved as a result of the geometric nonlinearity of DSIS. At the input of small amplitude loading, the isolation efficiency of DSIS can be enhanced by the loading rings, while at the large amplitude loading input, the isolation efficiency of DSIS can be ensured by its geometric nonlinearity. As a result, DSIS with loading rings can obtain a more comprehensive capacity to isolate vertical vibration.

Taking an in-situ test train-induced vibration as input, an analysis of the two DSIS was conducted [15]. The Main frequency range of the input train-induced vibration is about 30Hz–200Hz. According to the preceding transfer function analysis, the frequency of DSIS without loading rings affected by Coulomb friction is about 36Hz, which means that if the disc springs are combined in parallel, the DSIS without loading rings cannot effectively isolate the train-induced vibration. The comparison of the analysis is shown in Fig. 33. By setting loading rings, DSIS can significantly enhance the isolation abilities of the system, which benefit

from a lower start frequency of DSIS with loading rings. Thus, the effectiveness of the loading rings on the train-induced vibration is demonstrated.

6. Conclusion

A nonlinear vertical isolation system DSIS was explored. By setting the loading rings between the disc springs, a performance-improved DSIS was proposed. A calculation model for DSIS was proposed and experiments about DSIS were carried out too. In addition, a solution method for dynamic analysis was investigated using the proposed FC model. The conclusion from the theoretical and experimental studies are summarized as follows:

1. By considering the influence of the Coulomb friction, a calculation model with a form of piecewise function was presented. And the FC

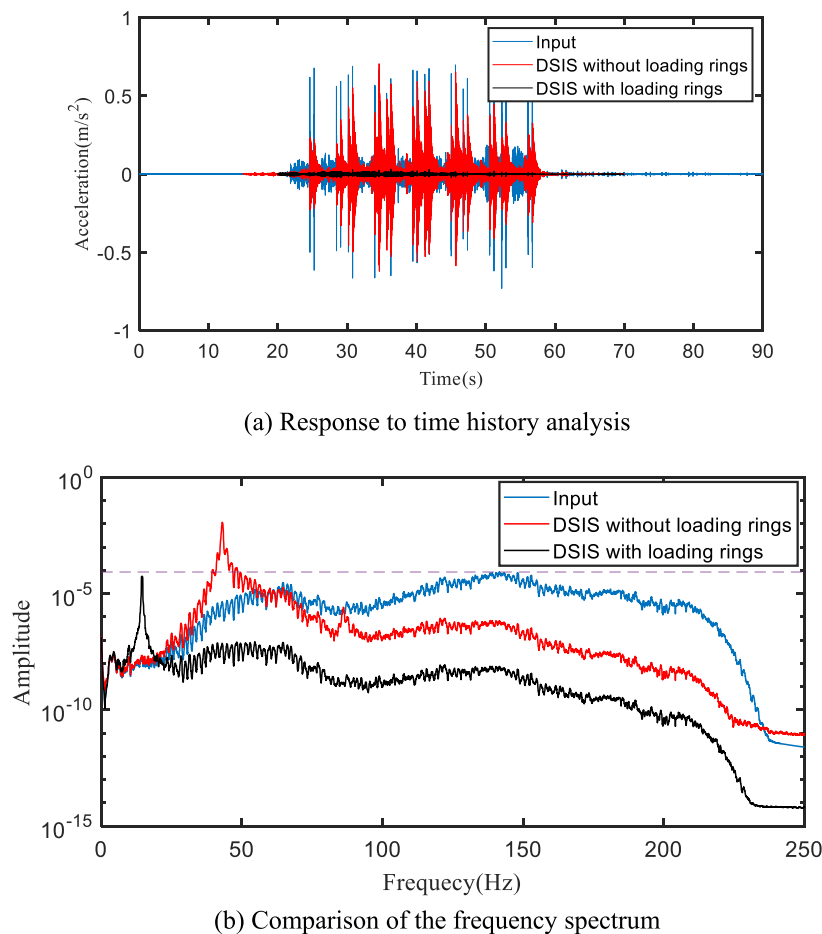


Fig. 33. Response of DSIS under train-induced vibration.

- model could describe the effect of Coulomb friction and the slip of the contact interface between the disc spring and loadings rings.
2. A series of tests were conducted to demonstrate the effect of loading rings. Experiment results showed that the DSIS with loading rings could significantly reduce the effect of the Coulomb friction. Especially, the loading rings could decrease the stiffness of the transition section obviously, which could enhance the isolation ability of DSIS.
 3. By comparing the experimental results with the calculation results based on the FC model, the accuracy of the presented model was verified. Thus, the presented FC model could effectively describe the force-displacement relation of DSIS.
 4. Based on the stepwise integration method, the solution method for the dynamic response of DSIS was studied. Through the proposed solution method, the dynamic response of DSIS was studied. The analysis results showed that setting the loading rings could significantly reduce the start frequency of DSIS and mainly improve the isolation efficiency of the small amplitude input. Therefore, DSIS could obtain a comprehensive reinforcement of the isolation capacity by setting loading rings.

Statement of author contribution

For the manuscript “Theoretical and experimental investigation on disc spring isolation system with loading rings”, there are three co-authors, who are Mr. Kaiqiang Ma, Prof. Ying Zhou, and Mr. Decheng Lu.

The first author Mr. Kaiqiang Ma a PhD candidate supervised by Prof. Ying Zhou. He carried out detailed work, including numerical analysis and experimental study, and wrote the manuscript.

The second author Prof. Ying Zhou has focused on the research of

nonlinear isolation systems for several years. Based on her abundant research and engineering experiences, she directed this research, conceived a new idea and revised the manuscript.

The third author Mr. Decheng Lu is a PhD candidate supervised by Prof. Zongyuan Yang. He helped to do the test and revised the manuscript.

The manuscript has already been reviewed by all authors and they all agree with the above description of the contribution of each one's work.

Declaration of competing interest

The authors declare that they have no known competing financial interests or personal relationships that could have appeared to influence the work reported in this paper.

Data availability

No data was used for the research described in the article.

Acknowledgements

The authors gratefully acknowledge the financial support from National Science Fund for Distinguished Young Scholars of China (Grant No. 52025083), National Natural Science Foundation of China (Grant No. 51878502), and Shanghai social development science and technology project(21DZ1203403).

References

- [1] Salazar AR, Haldar A. Structural responses considering the vertical component of earthquakes. *Comput Struct* 2000;74(2):131–45. [https://doi.org/10.1016/S0045-7949\(99\)00031-0](https://doi.org/10.1016/S0045-7949(99)00031-0).
- [2] Bas S, Kalkan I. The effects of vertical earthquake motion on an R/C structure. *Struct Eng Mech* 2016;59(4):719–37. <https://doi.org/10.12989/sem.2016.59.4.719>.
- [3] Bas S, Lee JH, Sevinc M, Kalkan I. Seismic performance of R/C structures under vertical ground motion. *Comput Concr* 2017;20(4):369–80. <https://doi.org/10.12989/cac.2017.20.4.369>.
- [4] Papazoglou AJ, Elnashai AS. Analytical and field evidence of the damaging effect of vertical earthquake ground motion. *Earthq Eng Struct Dynam* 1996;25:1109–37. [https://doi.org/10.1002/\(SICI\)1096-9845\(199610\)25:10<1109::AID-EQE604>3.0.CO;2-0](https://doi.org/10.1002/(SICI)1096-9845(199610)25:10<1109::AID-EQE604>3.0.CO;2-0).
- [5] Hesami S, Ahmadi S, Ghalesari AT. Numerical modeling of train-induced vibration of nearby multi-story building: a case study. *KSCE J Civ Eng* 2016;20(5):1701–13. <https://doi.org/10.1007/s12205-015-0264-9>.
- [6] Yonekawa Y, Maeda S, Kanada K, Takahashi Y. Whole-body vibration perception thresholds of recumbent subjects-Part 1: supine posture. *Ind Health* 1999;37(4):398–403. <https://doi.org/10.2486/indhealth.37.398>.
- [7] Zhang XH, Zhou SH, He C, Di HG, Si JB. Experimental investigation on train-induced vibration of the ground railway embankment and under-crossing subway tunnels. *Transp Geotech* 2021;26:100422. <https://doi.org/10.1016/j.trgeo.2020.100422>.
- [8] Noori B, Arcos R, Clot A, Romeu J. Control of ground-borne underground railway-induced vibration from double-deck tunnel infrastructures by means of dynamic vibration absorbers. *J Sound Vib* 2019;461:114914. <https://doi.org/10.1016/j.jsv.2019.114914>.
- [9] Tao ZY, Wang YM, Sanaye M, Moore JA, Zou C. Experimental study of train-induced vibration in over-track buildings in a metro depot. *Eng Struct* 2019;198:109473. <https://doi.org/10.1016/j.engstruct.2019.109473>.
- [10] Xia H, Zhang N, Cao YM. Experimental study of train-induced vibrations of environments and buildings. *J Sound Vib* 2005;280(3–5):1017–29. <https://doi.org/10.1016/j.jsv.2004.01.006>.
- [11] Araki Y, Asai T, Masui T. Vertical vibration isolator having piecewise-constant restoring force. *Earthq Eng Struct Dynam* 2009;38(13):1505–23. <https://doi.org/10.1002/eqe.915>.
- [12] Lombaert G, Degrande G, Vanhauwere B, Vandeborghi B, François S. The control of ground-borne vibrations from railway traffic by means of continuous floating slabs. *J Sound Vib* 2006;297:946–61. <https://doi.org/10.1016/j.jsv.2006.05.013>.
- [13] Fujita T. Earthquake isolation technology for industrial facilities—research, development and applications in Japan. *Bull N Z Soc Earthq Eng* 1985;18(3):224–49. <https://doi.org/10.5459/bnzsee.18.3.224-249>.
- [14] Pan P, Shen SD, Shen ZY, Gong RH. Experimental investigation on the effectiveness of laminated rubber bearings to isolate metro generated vibration. *Measurement* 2018;122:554–62. <https://doi.org/10.1016/j.measurement.2017.07.019>.
- [15] Zhou Y, Ma KQ, Chen P, Lu DC, Wu H. Investigations on train-induced vibration and vibration control of an over-track building using thick-layer rubber bearings. *Struct Des Tall and Spec* 2021;31:e1898. <https://doi.org/10.1002/tal.1898>.
- [16] Jiang YL, Song CS, Ding CM, Xu BH. Design of magnetic-air hybrid quasi-zero stiffness vibration isolation system. *J Sound Vib* 2020;477:115346. <https://doi.org/10.1016/j.jsv.2020.115346>.
- [17] Lan CC, Yang SA, Wu YS. Design and experiment of a compact quasi-zero-stiffness isolator capable of a wide range of loads. *J Sound Vib* 2014;333:4843–58. <https://doi.org/10.1016/j.jsv.2014.05.009>.
- [18] Araki Y, Kawabata S, Asai T, Masui T. Response of vibration-isolated object to ground motions with intense vertical accelerations. *Eng Struct* 2011;33(12):3610–9. <https://doi.org/10.1016/j.engstruct.2011.07.025>.
- [19] Kitayama S, Lee D, Constantinou MC, Kempner L. Probabilistic seismic assessment of seismically isolated electrical transformers considering vertical isolation and vertical ground motion. *Eng Struct* 2017;152(1):888–900. <https://doi.org/10.1016/j.engstruct.2017.10.009>.
- [20] Reyes SI, Almazán JL. A novel device for a vertical rocking isolation system with uplift allowed for industrial equipment and structures. *Eng Struct* 2020;214(1):110595. <https://doi.org/10.1016/j.engstruct.2020.110595>.
- [21] Carrella A, Brennan MJ, Waters TP. Static analysis of a passive vibration isolator with quasi-zero-stiffness characteristic. *J Sound Vib* 2007;301:678–89. <https://doi.org/10.1016/j.jsv.2006.10.011>.
- [22] Kovacic I, Brennan MJ, Waters TP. A study of a nonlinear vibration isolator with a quasi-zero stiffness characteristic. *J Sound Vib* 2008;315:700–11. <https://doi.org/10.1016/j.jsv.2007.12.019>.
- [23] Meng QG, Yang XF, Li W, Lu E, Sheng LC. Research and analysis of quasi-zero-stiffness isolator with geometric nonlinear damping. *Shock Vib* 2017;2017:6719054. <https://doi.org/10.1155/2017/6719054>.
- [24] Zhou XH, Sun X, Zhao DX, Yang X, Tang KH. The design and analysis of a novel passive quasi-zero stiffness vibration isolator. *J Vib Eng Technol* 2021;9:225–45. <https://doi.org/10.1007/s42417-020-00221-6>.
- [25] Meng LS, Sun JG, Wu WJ. Theoretical design and characteristics analysis of a quasi-zero stiffness isolator using a disk spring as negative stiffness element. *Shock Vib* 2015;2015:813763. <https://doi.org/10.1155/2015/813763>.
- [26] Zhou Y, Chen P, Mosqueda G. Analytical and numerical investigation of quasi-zero stiffness vertical isolation system. *J Eng Mech* 2019;145(6):04019035. [https://doi.org/10.1061/\(ASCE\)EM.1943-7889.0001611](https://doi.org/10.1061/(ASCE)EM.1943-7889.0001611).
- [27] Zhou Y, Chen P, Mosqueda G. Numerical studies of three-dimensional isolated structures with vertical quasi-zero stiffness property. *J Earthq Eng* 2021;26(7):3601–22. <https://doi.org/10.1080/13632469.2020.1813662>.
- [28] Zhou Y, Chen P. Investigations on a vertical isolation system with quasi-zero stiffness property. *Smart Struct Syst* 2020;25(5):543–57. <https://doi.org/10.12989/ssy.2020.25.5.543>.
- [29] Fang J, Dong H. Design of an improved nonlinear disc spring vibration isolator. *Appl Mech Mater* 2016;835:643–8. <https://doi.org/10.4028/www.scientific.net/AMM.835.643>.
- [30] Wang W, Wang XX. Tests, model, and applications for coned-disc-spring vertical isolation bearings. *Bull Earthq Eng* 2020;18:357–98. <https://doi.org/10.1007/s10518-019-00728-8>.
- [31] Wang W, Wang XX, Li AQ. Coned disc spring compound vertical isolation: testing and modelling. *J Earthq Eng* 2020. <https://doi.org/10.1080/13632469.2020.1850573>.
- [32] Zhou JC, Zhang CZ, Wang ZQ, Mao KM, Wang XY. A study on the influence of different constraint modes and number of disc springs on the dynamics of disc spring system. *Shock Vib* 2021;2021:8866159. <https://doi.org/10.1155/2021/8866159>.
- [33] Curti G, Montanini R. On the influence of friction in the calculation of conical disk springs. *J Mech Des* 1999;121(4):622–7. <https://doi.org/10.1115/1.2829508>.
- [34] Ozaki S, Tsuda K, Tominaga J. Analyses of static and dynamic behavior of coned disk springs: effects of friction boundaries. *Thin-Walled Struct* 2012;59:132–43. <https://doi.org/10.1016/j.tws.2012.06.001>.
- [35] Almen JO, Laszlo A. The uniform-section disk spring. *Trans Am Soc Mech Eng* 1936;58:305–14. <https://www.shopteener.com/library/pdf/193500.pdf>.
- [36] Jia F, Xu FY. Combined vibration isolator of disc springs for closed high-speed precision press: design and experiments. *Trans Can Soc Mech Eng* 2014;38(4):465–85. <https://doi.org/10.1139/tcsme-2014-0031>.
- [37] GAOQIAO. Disc spring(GB/T1972-2005). China [in Chinese]. <http://c.gb688.cn/bzgk/gb/showGb?type=online&hcno=8E249592C497ED5A2C62563B38C402DB>; 2005.
- [38] Warn GP, Whittaker AS. A study of the coupled horizontal-vertical behavior of elastomeric and lead-rubber seismic isolation bearings. New York, USA: University at Buffalo, The State University of New York; 2006. Technical Report MCEER-06-001, <https://ubir.buffalo.edu/xmlui/bitstream/handle/10477/25225/06-0011.pdf?sequence=3&isAllowed=y>.